

**Title: 18F-FDG PET/MRI in Chronic Sciatica: Early Results
Revealing Spinal and Non-spinal Abnormalities.**

Authors: Peter W. Cipriano^{1*}, Daehyun Yoon^{1*}, Harsh Gandhi¹, Dawn Holley¹,
Dushyant Thakur¹, Brian A. Hargreaves¹, David J. Kennedy², Matthew W.
Smuck², Ivan Cheng² and Sandip Biswal¹.

¹Department of Radiology, Stanford University School of Medicine, Stanford, CA.

²Department of Orthopaedics, Stanford University School of Medicine, Stanford,
CA

Financial support: This study is funded in part by General Electric Healthcare.

Corresponding author: Sandip Biswal MD

Address: 300 Pasteur Drive S-068B, Stanford, California 94305.

Phone number: 650-721-7382

Fax number: 650-725-7296

Email: biswal@stanford.edu.

***Co-first authors:** Peter Cipriano (BA, student) and Daehyun Yoon (Ph.D.,
research associate) are co-1st authors.

Running title: 18F-FDG PET/MRI in Chronic Sciatica

Peter Cipriano BA

Address: 1201 Welch Road, Stanford, California 94305.

Phone number: 650-721-7382

Fax number: 650-725-7296

Email: pciprian@stanford.edu.

Daehyun Yoon Ph.D.

Address: 3155 Porter Drive, Palo Alto, California 94304.

Phone number: 650-725-0452

Fax number: 650-498-5876

Email: quann@stanford.edu.

Word Count: 4,646

ABSTRACT

Chronic sciatica is a major cause of disability worldwide, but accurate diagnosis of the offending pathology remains challenging. In this report, the feasibility of a fluorodeoxyglucose (18F-FDG) positron emission tomography/magnetic resonance imaging (PET/MRI) approach for improved diagnosis of chronic sciatica is presented. **Methods:** 18F-FDG PET/MRI was performed on 9 chronic sciatica patients and 5 healthy volunteers. Region-of-interest analysis using maximum standardized uptake values (SUV_{max}) was performed, and 18F-FDG uptake in lesions was compared with the corresponding areas in healthy controls. **Results:** Significantly increased 18F-FDG uptake was observed in detected lesions of all patients, which was correlated with pain symptoms. 18F-FDG-avid lesions were not only found in impinged spinal nerves, but were also associated with non-spinal causes, such as a facet joint degeneration, pars defect, or a presumed scar neuroma. **Conclusion:** The feasibility of 18F-FDG PET/MRI for diagnosing pain generators in chronic sciatica has been demonstrated, revealing various possible etiologies.

Key Words: 18F-FDG; PET/MRI; sciatica; pain

INTRODUCTION

Sciatica is pain radiating from the buttock or lower back downward along the sciatic nerve into one or, less frequently, both legs (1). The most common cause of sciatica is a herniated intervertebral disc impinging upon a lumbar spinal nerve (2). However, a wide variety of other spinal and non-spinal causes have been implicated as the source of sciatica (3-5). Accordingly, determining the source of chronic sciatica remains challenging with current diagnostic methods. Sciatica becomes chronic in an estimated 20 to 30 percent of patients with the disease (6), and invasive treatments may be required for pain relief. Therefore, accurate identification of the pain source is essential to guide appropriate interventions.

No clinical test has been established that offers both high sensitivity and specificity in identifying the source of sciatica (7). History taking and physical examination are routinely performed, but their function is limited in identifying the source of pain (1,6). Electromyography may identify muscular denervation and isolate the injury to a specific spinal nerve (8). However, electromyography requires painfully invasive needle electrode insertion, and the sampling and interpretation process can be biased from the practitioner's skills (9). While MRI is currently the imaging modality of choice for sciatica diagnosis, its findings often do not correlate with symptoms. For example, the abnormal disc morphology on MRI can be indistinguishable between chronic sciatica patients and those whose sciatica has resolved (10).

Simultaneous 18F-FDG PET/MRI is a novel diagnostic approach that can offer metabolic and structural examination of painful lesions. Simultaneous acquisition of PET and MRI can greatly mitigate motion-induced mis-registration compared to separate acquisition with each modality. This is a significant advantage in specifying pain sources because the common sources of sciatic pain, such as herniated disc, degenerated facet joints, and impinged spinal nerves are located very closely to one another. The high sensitivity of 18F-FDG PET to metabolically hyperactive foci can be used to detect abnormal increase of metabolism caused by painful inflammation. A recent PET imaging study demonstrated increased 18F-FDG uptake in injured nerves of rats as well as in the denervated calf musculature on the affected limb (11). Unfortunately, the low spatial resolution and lack of tissue contrast in PET limit distinction between multiple possible pathologies in the detected lesion. High-resolution anatomy with superior soft-tissue contrast in MRI can help to resolve this anatomic ambiguity on PET (12). On the other hand, when multiple or subtle structural abnormalities are detected on MRI, the metabolic contrast in PET can highlight the pain-relevant inflammatory changes within the detected lesions.

The study aims to investigate the feasibility of whole-body 18F-FDG PET/MRI as a diagnostic tool to visualize the hypermetabolic and inflamed pathology in chronic sciatica. We performed whole-body 18F-FDG PET/MRI on chronic sciatica patients and asymptomatic controls, and compared the 18F-FDG uptake patterns between these groups.

MATERIALS AND METHODS

Patient Population

The Stanford University institutional review board approved our prospective observational study, and all subjects (both patients and controls) signed a written informed consent form. All data were collected in compliance with the Health Insurance Portability and Accountability Act. The clinical trial registration number of this study is NCT03195270. Nine patients presenting with chronic sciatica symptoms (unilateral leg pain greater than back pain for at least 3 months) were recruited for the patient group (5 men and 4 women; mean age \pm standard deviation, 38.2 ± 12.7 y; age range, 21-58y). All patients had at least a pain score of 4 on a 10 cm Visual Analog Scale at the time of imaging where 0 cm is no pain, and 10 cm is the worst pain imaginable. We also performed ^{18}F -FDG PET/MRI on five asymptomatic volunteers, who served as the control group (2 men and 3 women; mean age \pm standard deviation, 34.2 ± 8.4 y; age range, 22-48y).

PET/MR Imaging Process

All subjects fasted for at least four hours prior to the imaging session to ensure a blood glucose level below 180 mg/dL at the time of imaging. The mean and standard deviation of the administered activity of ^{18}F -FDG across patients and controls were 362.6 ± 17.7 MBq (range, 327.7-380.5MBq) and 359.5 ± 26.7

MBq (range, 318.8-389.3 MBq), respectively. The mean and standard deviation of administered activity normalized to body weight across patients and controls were 4.59 ± 0.63 MBq/kg (range, 4.38-6.08 MBq/kg) and 4.22 ± 1.13 MBq/kg (range, 3.75-6.58 MBq/kg), respectively. One hour after a single bolus injection of ^{18}F -FDG, subjects underwent PET/MR imaging in a GE PET/MRI scanner (SIGNA PET/MR, GE Healthcare, Waukesha, WI, USA). Subjects were scanned from the head to the feet in 8 to 10 bed positions for 1 to 1.5 hours, depending on the height of the patient. PET images were reconstructed with product reconstruction software using MR-based attenuation correction techniques (13-15). A common color scale ranging from 0 to 3 for SUV was used to render all the PET images.

The following MRI sequences were performed simultaneously with PET scans in each bed: 3D coronal double-echo steady-state (TR: 18.7ms, TE: 8.1ms, resolution: 1.2x1.2x2mm, flip angle: 30°), 3D axial liver imaging with volume acceleration-flexible (TR: 4.6ms, TE: 1.8ms, resolution: 1.3x1.3x3.4mm, flip angle: 15°), 3D axial double-echo steady-state (TR: 18.3ms, TE: 6.4ms, resolution: 0.7x0.7x2mm, flip angle: 30°), and 2D axial T2-weighted fast spin-echo with fat-saturation (TR: 5s, TE: 76ms, resolution: 1x1x2mm, echo train length: 8). For signal reception, a 16-channel head-neck coil, an integrated spine coil, and two 32-channel body phase-array coils were used.

Analysis of ^{18}F -FDG PET/MRI Images

We performed image analysis to identify 18F-FDG PET/MRI abnormalities by comparison with the contralateral side and with the control subjects. We first conducted a radiologic review of PET/MR images from patients to detect the lesions likely causing their symptoms. Two radiologists performed the review to identify structural abnormalities on MRI and/or focal hotspots on PET. Hotspot detection was based on the asymmetry of the 18F-FDG uptake or qualitative comparison with the imaging pattern of the controls. No patient information was used during the review to avoid any bias in detection of abnormalities. Rigorously validating the pain-relevance of detected abnormalities requires the direct treatment of those abnormalities and the evaluation of pain-relief outcome, which is beyond the scope of this research. In our study, we simply compared the side (left/right) of the reported pain with the side of the identified abnormalities.

To categorize lesions in the lumbar spine, we performed a region-of-interest analysis for 18F-FDG uptake by segmenting the following five areas at each lumbar spine level (L1 to L5) based on co-registered MRI anatomy: disc, lateral recess, neuroforamen, facet joint, and paraspinal muscle. We used Osirix (ver. 8.0, Pixmeo SARL, Switzerland) for the image segmentation and SUV measurement. To establish baseline measurements of 18F-FDG uptake, we calculated the mean and standard deviation of the SUV_{max} in those same segmented areas of the control subjects. For all detected lesions, both spinal and non-spinal, we measured the SUV_{max} and compared it with the contralateral

SUV_{max}.

For the lesions of a spinal nerve impingement due to a herniated disc (the most common cause of sciatica), the SUV_{max} was obtained from the lesion itself, the equivalent location on the contralateral side, and in the corresponding location in control subjects. These values were compared using the Mann-Whitney U-test to determine statistical significance ($p < 0.01$).

RESULTS

MRI Abnormalities

Spinal nerve impingement due to a herniated disc was detected in 6 out of 9 patients, and none of the nerve impingement was bidirectional, as summarized in Table 1. All impingements occurred at the L5-S1 vertebral level where, except for one case in which the impingement occurred at L4-L5 level. In the remaining three patients, bilateral L5 pars defects with L4-S1 spinal nerve neuritis, S2 peripheral nerve entrapment by the piriformis muscle, and bilateral L5-S1 facet arthropathy were identified.

18F-FDG Uptake in Lumbar Spine of Asymptomatic Controls

The mean and standard deviation of 18F-FDG SUV_{max} in segmented tissues at different levels of the lumbar spine from the 5 controls are introduced in Table 2. The average SUV_{max} of neuroforamen and facet joints were generally between 1.0 and 1.2. The SUV_{max} averages of disc, lateral recess, and

paraspinal muscle were mostly distributed between 0.6 and 0.8. These values served as a baseline in visual recognition of the 18F-FDG hotspots in patients during the radiologic review.

18F-FDG PET Abnormalities

Focally increased 18F-FDG PET uptake was found in both spinal and non-spinal tissues, as described in Table 2. In patients 1 through 5, abnormally high SUV_{max} ranging from 1.26 to 1.75 were identified on the lateral recess at the L5-S1 level, except for patient 4 (L4-L5). The co-registration of MRI revealed that these lateral recesses were narrowed due to disc herniation. In all cases, SUV_{max} of these lesions were higher than the SUV_{max} of the contralateral side, as shown in Fig. 1A. The SUV_{max} difference between the two sides was the smallest in patient 3, where subtle compression was observed in the contralateral spinal nerve as well. Note that the SUV_{max} of lesions and contralateral sides were higher than the mean SUV_{max} of controls (green dotted line). Because the PET/MRI lesions were found at L4-S1 levels, the mean SUV_{max} of controls was calculated from the same levels. Fig. 1B compares the distributions of SUV_{max} in Fig. 1A. The p-values from the Mann-Whitney U-test of SUV_{max} in lesions against SUV_{max} in contralateral sides and controls were all less than 0.01, indicating a significant difference in their medians. Patients 1 through 5 also demonstrated high 18F-FDG uptake in leg muscles, including the biceps femoris, extensor hallucis longus, soleus and tibialis anterior muscles ipsilateral to the side of disc herniation. The SUV_{max} of these muscles ranged from 1.0 to 2.5, higher than the

contralateral SUV_{max} by 15% to 96%.

In patients 6 through 9, no high 18F-FDG uptake was detected in the lateral recesses of the lumbar spine. Instead, the 18F-FDG uptake abnormalities were found in the following locations, respectively: the S2 peripheral nerve entrapped by the piriformis muscle (SUV_{max} 1.4), a focal spot in the left calf muscles (SUV_{max} 1.84), the left L5-S1 facet joint (SUV_{max} 2.94), the left hamstring tendon (SUV_{max} 2.1), and the L5 pars defect (SUV_{max} 1.3). The SUV_{max} in these areas was higher than the contralateral SUV_{max} by 14% to 54%.

Relevance of PET/MRI Abnormalities to Pain Symptoms

In patients 1 through 5, both MRI and 18F-FDG PET showed abnormalities at the lateral recess on the side ipsilateral to the patient's pain symptom. More specifically, asymmetrically high 18F-FDG uptake co-localized to the herniated disc and the adjacent compressed spinal nerve was observed with MRI. These same 5 patients also showed increased 18F-FDG uptake in their leg ipsilateral to site of symptoms, whereas the corresponding MRI of the same leg did not show any signal or structural abnormalities. Fig. 2 depicts a representative case among these patients. The axial MR image (Fig. 2A) shows the descending right S1 spinal nerve impinged by focal protrusion of the L5-S1 disc (yellow arrow) with abnormally increased SUV_{max} (yellow arrow, Fig. 2C) compared to the contralateral side (1.66 vs 1.08). Fig. 1D shows the coronal MR image of both legs of the same patient, showing no structural abnormality. The

coronal PET image (Fig. 2E), however, presents abnormal 18F-FDG uptake in the biceps femoris muscle (red arrow). The SUV_{max} of this muscle was 1.39, much higher than the contralateral SUV_{max} (0.85) (Fig. 1F). In patient 6, the MRI and PET abnormalities were detected on the same area ipsilateral to the patient's pain as well, but they were in the non-spinal areas (S2 peripheral nerve).

In patients 7 through 9, the sides of detected MRI abnormalities were not always on the same side of the patient's pain. Fig. 3 introduces the case of patient 7, in which the MRI abnormality was detected on the side opposite the patient's pain. The MR image (Fig. 3A) shows the impinged S1 spinal nerve in the right lateral recess (green arrow), but the patient's pain was *left-sided*. Interestingly, no significant 18F-FDG uptake was observed at either lateral recess (Fig. 3B), or at any vertebral level of the lumbar spine. While MRI of the lower extremities showed no structural abnormalities (Fig. 3C), a discrete focus of high 18F-FDG uptake ($SUV_{max} = 1.84$) was found between the left gastrocnemius and soleus muscles (Fig. 3D). In this region of high 18F-FDG uptake, the patient reported a superficial area of numbness. The corresponding location on the contralateral limb yielded a substantially lower SUV_{max} (0.84), and the patient did not report numbness in this area. The medical history of the patient revealed a direct traumatic blow to the region from a skiing accident. We suspect the image abnormality to be a scar neuroma that resulted from the accident, causing the local skin numbness and the leg pain.

In each of patients 8 and 9, the MRI abnormality was detected bilaterally, whereas the PET abnormality was detected only on the side ipsilateral to the pain. Fig. 4 illustrates the case of patient 8, in which the axial MR image (Fig. 4A) shows mildly hypertrophied and osteophytic facet joints bilaterally at the L5-S1 level. Note that this MR finding was not convincing to assure its contribution to the patient's symptom. However, a very significant ^{18}F -FDG uptake (white arrows, $\text{SUV}_{\text{max}} = 2.94$) was observed around the left L5-S1 facet joint ipsilateral to the patient's pain (Fig. 4B), boosting the likelihood of the left L5-S1 facet joint being the source of pain, rather than the right facet joint.

DISCUSSION

In this study, we present ^{18}F -FDG PET/MRI findings of nine chronic sciatica cases to demonstrate the feasibility of our ^{18}F -FDG PET/MRI approach for locating the source of sciatica. In 5 out of 9 patients, spinal nerve impingement due to a herniated disc was identified as a relevant lesion based on both MRI morphology and high ^{18}F -FDG uptake. In the remaining 4 patients, different types of lesions were found in the leg muscles, peripheral nerve, pars, and facet joints, where ^{18}F -FDG uptake was abnormally high but only mild abnormalities or no abnormalities appeared in MRI.

The complementary combination of the metabolic interrogation by ^{18}F -FDG PET and anatomic localization by 3T MRI showed potential for improved

identification of the sciatic pain sources in a limited number of sciatica patients. For example, the morphologic findings on MRI could contribute to specifying the type of lesion detected by PET for the spinal nerve root impingement case in Fig. 1. The high ^{18}F -FDG uptake may indicate a potentially painful lesion but, in the absence of MRI, cannot specify the lesion type among possible local pathologies, such as tumor, facet synovitis, disc herniation or other causes of an impinged spinal nerve. By co-registering the PET and MR images, the lesion was specifically identified as spinal nerve impingement by a herniated disc. Our results also demonstrated a case (Fig. 3) that focal, increased ^{18}F -FDG uptake can help delineate the pain-relevant pathology when multiple structural abnormalities are observed on MRI. The radiologic review of the MR image without the patient information suggested the descending right S1 spinal nerve impingement might cause sciatic nerve pain on the right side. However, this is a false-positive finding because the patient's pain was on the contralateral side. Evaluation of the ^{18}F -FDG PET/MRI image demonstrated a lack of ^{18}F -FDG uptake in this protruding disc and impinged nerve, thus decreasing the importance of this MR finding.

The high ^{18}F -FDG uptake observed in the leg muscles without any structural abnormalities in MRI suggest a few possible etiologies of one's sciatica. First, the patient may actually have a herniated disc and nerve impingement. This injury to the nerve is known to give rise to downstream neuropathic changes in muscle, including edema or atrophy. A second possibility

is that the abnormal ^{18}F -FDG uptake in the muscle may reflect a primary problem with the muscle (e.g., infectious or non-infectious myositis, ischemia, trauma), thus mimicking symptoms of spinal sciatica. In this case, a diagnostic local anesthetic injection to the foci of the high ^{18}F -FDG uptake in the muscle may be useful to confirm or refute the peripheral pain source. A third possible reason for abnormal muscular uptake of ^{18}F -FDG is that altered mechanics to accommodate or minimize painful conditions will result in the recruitment of muscles that are not necessarily pain generators (e.g., gait-alteration or limp). We believe a longitudinal study of a larger patient population is required to rigorously classify and validate these potential non-spinal sources of sciatica.

Our whole-body imaging approach allows for the investigation of potential abnormalities in other body parts that may differentiate sciatica patients from asymptomatic controls. While we observed both spinal and non-spinal manifestations of disease in sciatica patients, a more systematic search would be needed to determine the involvement of other body structures in the disease. For example, the quantitative correlation of the ^{18}F -FDG PET/MRI pattern in the central nervous system with the symptoms and detected abnormalities in the lower extremities would be an interesting topic for future research. Note that, in asymptomatic controls, we often observed a higher-than-background ^{18}F -FDG uptake pattern in the extensor compartment of both forearms (SUV_{max} ranging from 0.5 to 4.2). We suspect this is due to mechanical recruitment of these muscles, either just prior to or during injection of the radiotracer, despite our

efforts to keep the patients in a relaxed position. Another common, non-specific pattern in asymptomatic controls was the high ^{18}F -FDG uptake in the anterior compartment muscles of the lower legs (SUV_{max} ranging from 0.5 to 3 in anterior tibialis, extensor digitorum longus, and extensor hallucis longus muscles). We suspect this is also due to mechanical recruitment of these muscles immediately prior to or during the injection of ^{18}F -FDG.

This study is limited by the small size of the patient and control populations as well as potential selection bias in patients due to their chronic condition. Although the results are encouraging, our findings are based on the imaging results from only nine sciatica patients and five asymptomatic controls. Therefore, the investigation of a larger cohort of patients should be followed to robustly determine ^{18}F -FDG PET/MRI phenotypes of chronic sciatica. For future studies, MRI sequences could be customized to improve the value of MRI beyond anatomical investigation. For example, diffusion MRI techniques for the evaluation of spinal nerve compression (16-18) have shown promising results. Lastly, following the course of treatment for patients after our PET/MRI study can provide the data to evaluate the predictive value of these image findings and their contribution to the treatment options.

CONCLUSION

We present a novel ^{18}F -FDG PET/MRI approach for diagnosing the source of chronic sciatica. Our approach demonstrated the feasibility of

examining spinal and non-spinal sources with respect to tissue metabolism and anatomy. A follow-up study on a larger patient population is required to validate the clinical impact of the proposed method.

ACKNOWLEDGEMENTS

We thank Ms. Ma A. Ith for coordinating the patient recruitment process and Dr. Deepak Behera for his initial efforts in setting up the study protocol.

REFERENCES

1. Ropper AH, Zafonte RD. Sciatica. *N Engl J Med*. 2015;372:1240-1248.
2. Mixer WJ, Barr JS. Rupture of the intervertebral disc with involvement of the spinal canal. *N Engl J Med*. 1934;211:210-215.
3. Visser LH, Nijssen PG, Tijssen CC, van Middendorp JJ, Schieving J. Sciatica-like symptoms and the sacroiliac joint: clinical features and differential diagnosis. *Eur Spine J*. 2013;22:1657-1664.
4. Kirschner JS, Foye PM, Cole JL. Piriformis syndrome, diagnosis and treatment. *Muscle Nerve*. 2009;40:10-18.
5. Ergun T, Lakadamyali H. CT and MRI in the evaluation of extraspinal sciatica. *Br J Radiol*. 2010;83:791-803.
6. Koes BW, van Tulder MW, Peul WC. Diagnosis and treatment of sciatica. *BMJ*. 2007;334:1313-1317.
7. van der Windt DA, Simons E, Riphagen, II, et al. Physical examination for lumbar radiculopathy due to disc herniation in patients with low-back pain. *Cochrane Database Syst Rev*. 2010:CD007431.
8. Lewis AM, Layzer R, Engstrom JW, Barbaro NM, Chin CT. Magnetic resonance neurography in extraspinal sciatica. *Arch Neurol*. 2006;63:1469-1472.
9. Haig AJ, Yamakawa K, Kendall R, Miner J, Parres CM, Harris M. Assessment of the validity of masking in electrodiagnostic research. *Am J Phys Med Rehabil*. 2006;85:475-481.
10. el Barzouhi A, Vleggeert-Lankamp CL, Lycklama a Nijeholt GJ, et al. Magnetic resonance imaging in follow-up assessment of sciatica. *N Engl J Med*. 2013;368:999-1007.
11. Behera D, Jacobs KE, Behera S, Rosenberg J, Biswal S. (18)F-FDG PET/MRI can be used to identify injured peripheral nerves in a model of neuropathic pain. *J Nucl Med*. 2011;52:1308-1312.

- 12.** Biswal S, Behera D, Yoon DH, et al. [18F]FDG PET/MRI of patients with chronic pain alters management: early experience. *EJNMMI Phys.* 2015;2:A84.
- 13.** Sekine T, Buck A, Delso G, et al. Evaluation of atlas-based attenuation correction for integrated PET/MR in human brain: application of a head atlas and comparison to true CT-based attenuation correction. *J Nucl Med.* 2016;57:215-220.
- 14.** Wollenweber SD, Ambwani S, Lonn AHR, et al. Comparison of 4-class and continuous fat/water methods for whole-body, MR-based PET attenuation correction. *IEEE Trans Nucl Sci.* 2013;60:3391-3398.
- 15.** Wollenweber SD, Ambwani S, Delso G, et al. Evaluation of an atlas-based PET head attenuation correction using PET/CT & MR patient data. *IEEE Trans Nucl Sci.* 2013;60:3383-3390.
- 16.** Ailianou A, Fitsiori A, Syrogiannopoulou A, et al. Review of the principal extra spinal pathologies causing sciatica and new MRI approaches. *Br J Radiol.* 2012;85:672-681.
- 17.** Shi Y, Zong M, Xu X, et al. Diffusion tensor imaging with quantitative evaluation and fiber tractography of lumbar nerve roots in sciatica. *Eur J Radiol.* 2015;84:690-695.
- 18.** Zhou X, Cipriano P, Kim B, et al. Detection of nociceptive-related metabolic activity in the spinal cord of low back pain patients using 18F-FDG PET/CT. *Scand J Pain.* 15:53-57.

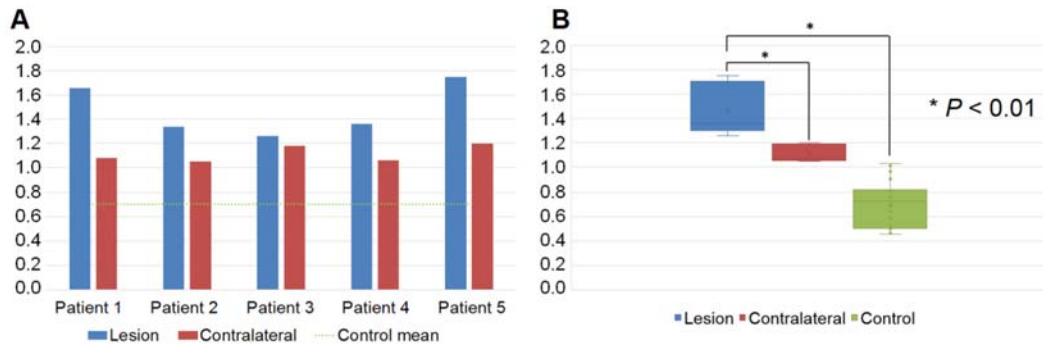


FIGURE 1. 18F-FDG SUV_{max} of lateral recess in lesions, contralateral side, and controls. (A) 18F-FDG SUV_{max} in lesions of an impinged spinal nerve due to a herniated disc and contralateral SUV_{max} from five patients. Mean SUV_{max} from controls are plotted in a green dotted line. (B) Distributions of 18F-FDG SUV_{max} of lesions, contralateral sides, and controls in (A). Mann-Whitney U-test demonstrated p-values less than 0.01 in the comparison of SUV_{max} between lesions and contralateral sides, and also in the comparison of SUV_{max} between lesions and controls.

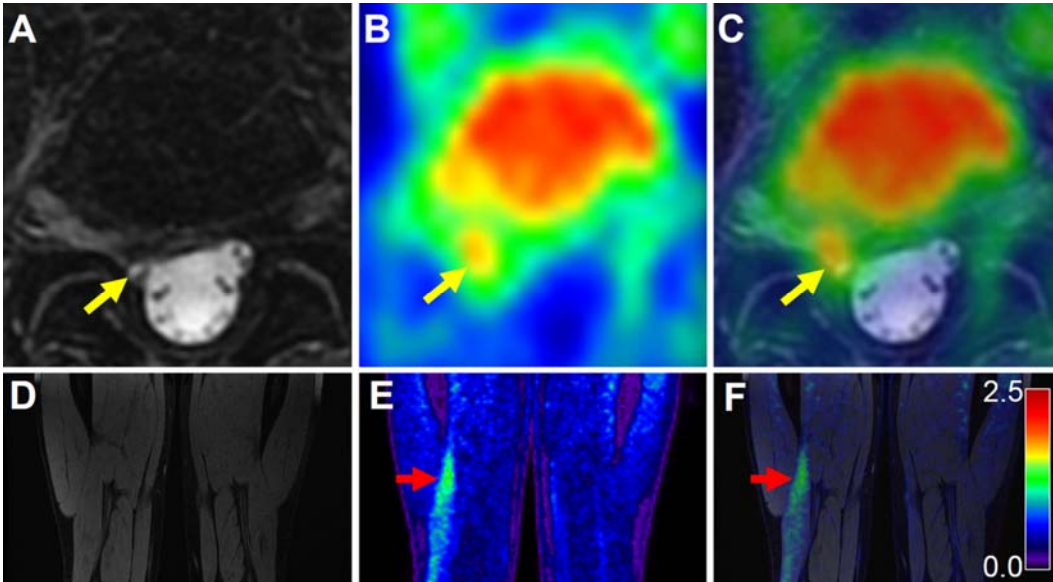


FIGURE 2. ¹⁸F-FDG PET/MRI findings of a right-sided sciatica patient with a spinal nerve impingement due to a herniated disc. (A) Axial T2-weighted fast spin echo MRI image showing a herniated disc at the L5-S1 level compressing the descending S1 spinal nerve in the right lateral recess (yellow arrow). (B) ¹⁸F-FDG PET image presenting asymmetrically increased ¹⁸F-FDG uptake on the right side. (C) ¹⁸F-FDG PET/MRI co-registered image displaying the increased uptake at the impinged S1 spinal nerve. (D) Coronal double echo steady-state MR image of the mid-thighs demonstrating no structural damage such as muscle atrophy or muscle edema from denervation. (E) ¹⁸F-FDG PET image illustrating high ¹⁸F-FDG uptake in the right leg. (F) ¹⁸F-FDG PET/MRI co-registered image showing high ¹⁸F-FDG uptake at the biceps femoris muscle. All PET images use the common color scale ranging from 0 to 2.5 for SUV as in the color bar in (E).

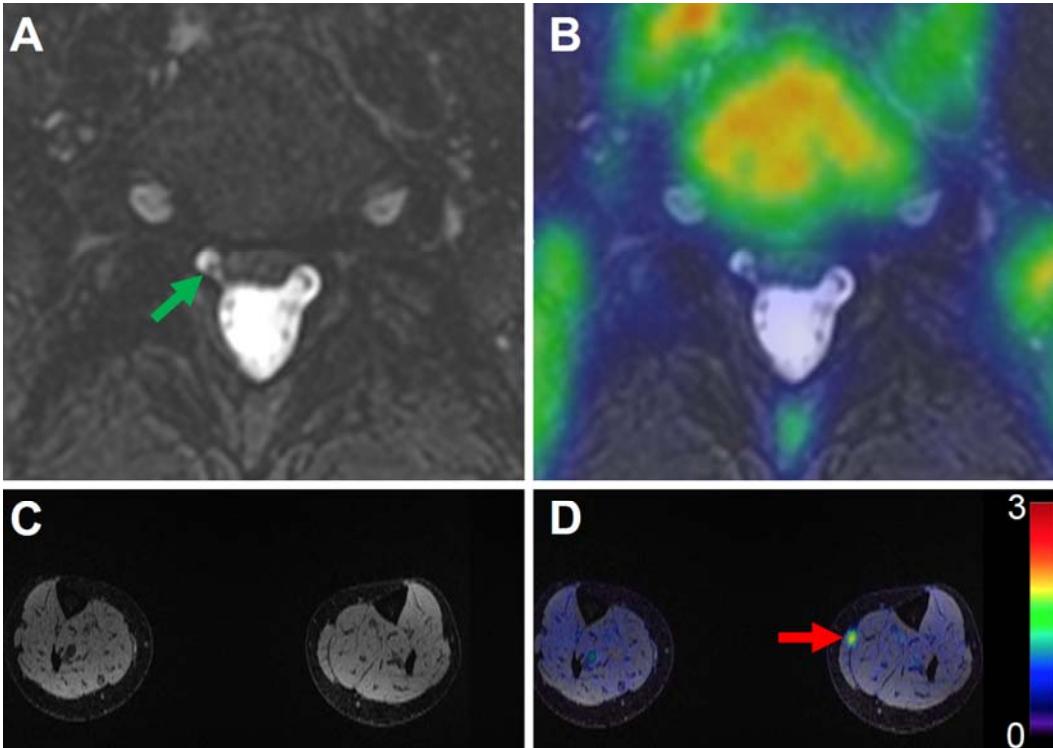


FIGURE 3. Different findings between ^{18}F -FDG PET and MRI of a left-sided sciatica patient. (A) Axial T2-weighted fast spin echo MRI image indicating that a right S1 spinal nerve is impinged by a herniated disc at the L5-S1 level (green arrow). This is not likely to be the cause of sciatica because the pain is on the other side. (B) ^{18}F -FDG PET/MRI co-registered image showing no asymmetrically increased ^{18}F -FDG uptake at the impinged spinal nerve compared to the contralateral side. (C) Axial double echo steady-state MR image of a lower leg (calf) revealing no structural degeneration or signal abnormality. (D) ^{18}F -FDG PET/MRI co-registered image demonstrating high ^{18}F -FDG uptake at the left gastrocnemius and soleus muscles (red arrow), where the patient reported skin numbness.

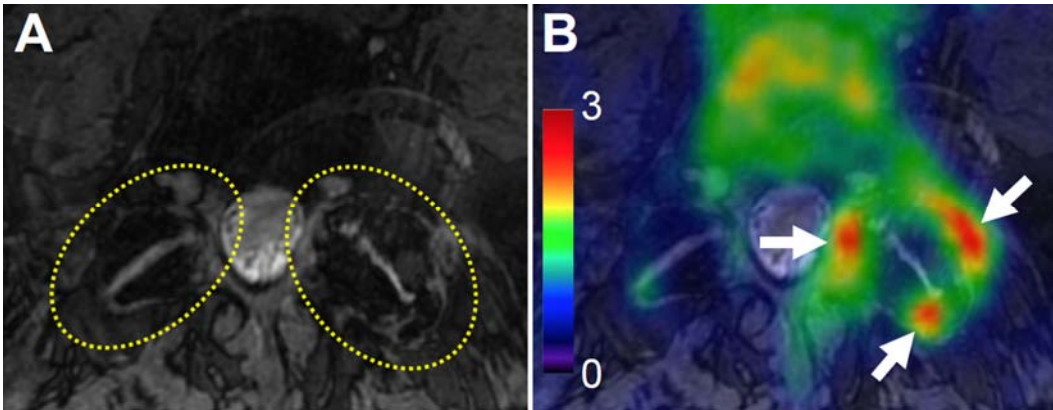


FIGURE 4. ¹⁸F-FDG PET/MRI findings of a left-sided sciatica patient with bilateral MRI abnormalities. (A) Axial double echo steady-state MR image showing degenerated L5-S1 facet joints bilaterally with a mild form of hypertrophy and osteophyte (yellow dotted circles). (B) ¹⁸F-FDG PET/MRI co-registered image, revealing the high ¹⁸F-FDG uptake to be around the degenerated L5-S1 facet joint on the left side only (white arrows).

TABLE 1

Abnormal 18F-FDG PET/MRI findings of patients

	Painful side	SUV_{max} of 18F-FDG (lesion / contralateral)	MRI abnormalities
Patient1	Right	Right L5-S1 lateral recess (1.66 / 1.08) Right biceps femoris muscle (1.39 / 0.85)	Compression of right S1 spinal nerve by disc bulge at L5-S1
Patient2	Right	Right L5-S1 lateral recess (1.34 / 1.05) Right biceps femoris muscle (1.00 / 0.51) Right extensor hallucis longus muscle (2.50 / 1.33)	Compression of right S1 spinal nerve by disc bulge at L5-S1
Patient3	Right	Right L5-S1 lateral recess (1.26 / 1.18) Right biceps femoris muscle (1.42 / 1.24)	Compression of right S1 spinal nerve by disc bulge at L5-S1
Patient4	Left	Left L4-L5 lateral recess (1.36 / 1.06) Left soleus muscle (1.10 / 0.84)	Compression of left L5 spinal nerve by disc bulge at L4-L5
Patient5	Right	Right L5-S1 lateral recess (1.75 / 1.20) Right tibialis anterior muscle (1.24 / 0.82)	Compression of right S1 spinal nerve by disc bulge at L5-S1
Patient6	Right	Right S2 peripheral nerve (1.4 / 1.2)	Entrapment of right S2 peripheral nerve by piriformis muscle
Patient7	Left	Left gastrocnemius and soleus muscle (1.84 / 0.84)	Mild compression of right S1 spinal nerve by disc bulge at L5-S1
Patient8	Left	Left L5-S1 facet joint (2.94 / 1.53) Left hamstring tendon (2.1 / 1.4)	Bilateral facet arthropathy at L5-S1
Patient9	Left	Left L5 pars (1.30 / 0.80)	Bilateral L5 pars defects, Neuritis on left L4-S1 spinal nerve

TABLE 2

mean \pm standard deviation of SUV_{max} in lumbar spine areas of controls

	L1/L2	L2/L3	L3/L4	L4/L5	L5/S1
Lateral recess	0.90 \pm 0.18	0.69 \pm 0.15	0.71 \pm 0.21	0.70 \pm 0.21	0.71 \pm 0.17
Neuroforamen	1.23 \pm 0.23	1.24 \pm 0.23	1.20 \pm 0.27	1.10 \pm 0.17	1.05 \pm 0.25
Disc	0.75 \pm 0.15	0.61 \pm 0.15	0.61 \pm 0.18	0.68 \pm 0.13	0.68 \pm 0.23
Facet joints	1.11 \pm 0.26	1.18 \pm 0.26	1.06 \pm 0.25	1.18 \pm 0.30	1.00 \pm 0.22
Paraspinal muscle	0.77 \pm 0.13	0.73 \pm 0.17	0.75 \pm 0.18	0.67 \pm 0.15	0.66 \pm 0.22